REPORT DOCUMENTATION PAGE

Form Approved
OMB No. 0704-0188

1. REPORT DATE *(DD-MM-YYYY)*	2. REPORT TYPE	3. DATES COVERED *(From - To)*
APRIL 2013	JOURNAL ARTICLE (POST PRINT)	SEP 2011 – SEP 2012

4. TITLE AND SUBTITLE

A COMPACT MODELING OF TIO2-TIO2-X MEMRISTOR

5a. CONTRACT NUMBER
FA8750-11-1-0271

5b. GRANT NUMBER

5c. PROGRAM ELEMENT NUMBER
62788F

6. AUTHOR(S)

Lu Zhang (UPitt), Zhijie Chen (UPitt), J. Joshua Yang (UPitt), Yiran Chen (UPitt), Bryant Wysocki (AFRL), and Nathan McDonald (AFRL)

5d. PROJECT NUMBER
T2NC

5e. TASK NUMBER
PI

5f. WORK UNIT NUMBER
TT

7. PERFORMING ORGANIZATION NAME(S) AND ADDRESS(ES)
Electrical and Computer Engineering Department
University of Pittsburgh
4200 Fifth Ave
Pittsburgh, PA 15213

8. PERFORMING ORGANIZATION REPORT NUMBER
N/A

9. SPONSORING/MONITORING AGENCY NAME(S) AND ADDRESS(ES)
Air Force Research Laboratory/Information Directorate
Rome Research Site/RITB
525 Brooks Road
Rome NY 13441-4505

10. SPONSOR/MONITOR'S ACRONYM(S)
AFRL/RI

11. SPONSORING/MONITORING AGENCY REPORT NUMBER
AFRL-RI-RS-TP-2013-013

12. DISTRIBUTION AVAILABILITY STATEMENT
APPROVED FOR PUBLIC RELEASE; DISTRIBUTION UNLIMITED. PA Case Number: 88ABW-2012-6207
DATE CLEARED: 28 November 2012

13. SUPPLEMENTARY NOTES

14. ABSTRACT
We developed a SPICE-compatible compact model of TiO2-TiO2-x memristors based on classic ion transportation theory. Our model is shown to simulate important dynamic memristive properties, e.g., the doping front motion and realtime memristance switching, which are critical in memristor-based analog circuit designs. The model, as well as its analytical approximation, is validated with the experimentally obtained data from real devices. Minor deviations of our model from the measured data are also analyzed and discussed.

15. SUBJECT TERMS
Memristor, TiO2-TiO2-x, campact model

16. SECURITY CLASSIFICATION OF:			17. LIMITATION OF ABSTRACT	18. NUMBER OF PAGES	19a. NAME OF RESPONSIBLE PERSON
a. REPORT	b. ABSTRACT	c. THIS PAGE			NATHAN MCDONALD
U	U	U	UU	05	19b. TELEPHONE NUMBER (*Include area code*) N/A

Standard Form 298 (Rev. 8-98)
Prescribed by ANSI Std. Z39.18

A compact modeling of TiO_2-TiO_{2-x} memristor

Lu Zhang,[1,a)] Zhijie Chen,[1] J. Joshua Yang,[2] Bryant Wysocki,[3] Nathan McDonald,[3] and Yiran Chen[1]
[1]*Department of Electrical and Computer Engineering, University of Pittsburgh, Pittsburgh, Pennsylvania 15261, USA*
[2]*HP Labs, Palo Alto, California 94304, USA*
[3]*U.S. Air Force Research Lab, Rome, New York 13440, USA*

(Received 8 January 2013; accepted 4 April 2013; published online 16 April 2013)

We developed a SPICE-compatible compact model of TiO_2-TiO_{2-x} memristors based on classic ion transportation theory. Our model is shown to simulate important dynamic memristive properties like real-time memristance switching, which are critical in memristor-based analog circuit designs. The model, as well as its analytical approximation, is validated with the experimentally obtained data from real devices. Minor deviations of our model from the measured data are also analyzed and discussed. © *2013 AIP Publishing LLC* [http://dx.doi.org/10.1063/1.4802206]

The operational characteristics of memristive devices are typically represented by an I-V curve: the memristance of the device changes with the magnitude and pulse duration of the externally applied excitations.[1] As one of the promising technologies, TiO_2-TiO_{2-x} memristor has recently received significant attention and been widely studied in the solid state device society.[2–10] Some physical models of memristive devices, such as HfO_x and NiO_x, proposed a general description on the switching on/off procedure based on the ion/vacancy motion driven by the electric field (or potential gradient), which is known as the filament formation or dissolution.[11–18] The behavior of the TiO_2-TiO_{2-x} device can also be understood by the similar ionic influence:[3,4,19–23] the filament corresponds to the high conductive region while the remaining regions can be treated as low conductive or insulating. Some other models present the understandings on internal state changes under physical factors like electric field and temperature.[11,12,24] Some previous work has proposed to model the memristive switching behavior in oxide devices based on the dynamical interactions between electrons, oxygen vacancies, and oxygen anions.[25] However, due to the high computation cost of complex physical quantities, i.e., transition Hamilton matrix and energy density of states, the model cannot be directly applicable to fast circuit simulation. By combining Monte-Carlo method, electron hopping conduction process can be simulated through the similar technique.[26] Kinetic Monte-Carlo method is also implemented to model the filament formation.[27] However, these models do not explicitly give the static and dynamic electrical switching properties of the memristor device. In some TiO_x memristor modeling works, the motion of vacancies is simulated through classical molecular dynamics.[28,29] The dynamics of tunnel barrier width can be also obtained by modeling the device as a resistor plus Simmons tunnel barrier.[30] In this work, we model the behavior of memristor device from classical macroscopic viewpoint, which is represented by the electron density distribution inside the device. A compact model of TiO_2-TiO_{2-x} memristor based on classic ion transportation theory is then proposed, targeting the application in SPICE circuit simulations. Compared to the aforementioned TiO_x memristor models, our model offers a concrete calculation of the filament dynamics and derives accurate time-varying behaviors of device resistance changing. Our model, as well as its analytical approximation, well matches the measurements of a real TiO_2-TiO_{2-x} device on static I-V curve and dynamic pulse programming.

We divide a TiO_2-TiO_{2-x} memristor into three regions, namely, the conductive region, the transition region, and the insulating region, as shown in Fig. 1. Here, the conductive region corresponds to the region of filaments while the transition region connects the filaments and the remaining insulating region. The formation or dissolution of the filament is simulated as the ion surface motion within the transition region. We use w, λ, and D to denote the lengths of the conductive region, the transition region, and the entire device, respectively. The real-time current density at position x in the memristor at time t can be expressed as[31]

$$J_s(x,t) = n_s(x,t)q\mu E_s(x,t) - qD_q\frac{dn_s(x,t)}{dx}. \quad (1)$$

Here, the subscript $s = (c, t, i)$ denotes the parameter of conductive region, transition region, and insulating region,

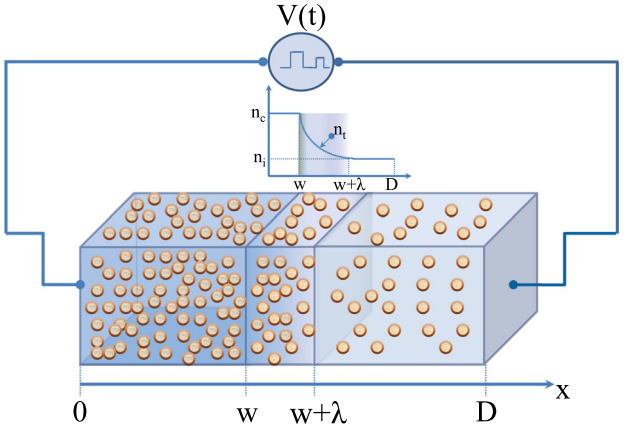

FIG. 1. Region partitioning of TiO_2-TiO_{2-x} memristor.

a)luz14@pitt.edu

respectively. E_s and n_s represent the electric field and the electron density, respectively. μ is the mobility coefficient. q is the elementary charge. D_q is the diffusion constant for electrons. Equation (1) shows that the current is generated mainly from the electron drifting in the electric field and the electron density gradient. D_q is typically small for electron diffusion current, and the second term in Eq. (1) is ignored in our model. If we ignore the variation of the cross section area and assume the current density is uniform in the memristor (i.e., $J_c = J_t = J_i$), the relationships between the electric fields and electron densities of the three regions can be summarized as

$$n_c q\mu E_c(t) = n_t(x,t) q\mu E_t(x,t) = n_i(t) q\mu E_i(t). \tag{2}$$

Here, we assume that the E_s and n_s are uniform in conductive and insulating regions and are determined only by the real-time applied voltage (except that n_c is a constant). The equation for the hopping rate of ions in a infinitely large lattice can be expressed as[32]

$$R = f \sinh(QEa/2kT) e^{-U/kT}, \tag{3}$$

where R is the ion hopping rate, f is the escape attempt frequency, a is the lattice periodicity, E is the electric field, Q is the charge of ion, U is the activation energy, k is the Boltzmann constant, and T is the local temperature. By considering the fact that the number of generated electrons is proportional to that of the hopping ions inside the thin film, we use the product of a coefficient γ_i and a factor $(n_c - n_i(t))$ to approximate the electron density generation function under the influence of electric field in the insulating region. $(n_c - n_i(t))$ also implies that the maximum electron density should not exceed n_c. Hence, the evolution of the electron density in insulating region under a time-varying electric field E_i can be calculated by

$$\frac{dn_i(t)}{dt} = \gamma_i (n_c - n_i(t)) E_i(t), \tag{4}$$

where γ_i is the electron density generating coefficient in the insulating region. At a given time t and position x, the electric field E_t can be viewed as a linear function bounded by E_c and E_i as

$$E_t(x,t) = \frac{(E_i(t) - E_c(t))}{\lambda}(x - w) + E_c(t). \tag{5}$$

We note that the voltage $V(t)$ applied on the two ends of the memristor equals the integral of the electric field along the device, or

$$V(t) = E_c(t) w + \int_w^{w+\lambda} E_t(x,t)dx + E_i(t)(D - \lambda - w). \tag{6}$$

Combining Eqs. (5) and (6), we have

$$E_c(t) = \frac{V(t)}{w + \frac{1}{2}\lambda + \frac{n_c}{n_i(t)}\left(D - w - \frac{1}{2}\lambda\right)}. \tag{7}$$

Finally, the transition region length λ reduces when the applied voltage $V(t)$ increases, which is approximated by

$$\lambda = \lambda_0 e^{-|V(t)|}, \tag{8}$$

in our model. λ_0 is the transition region length at $V(t) = 0$.

The probability of ion hopping changes with the external electric field.[32] However, the probability is significantly different in the conductive and insulating regions, which leading to the conductivity difference in these two regions. Ideally, every successful ion hopping produces two free electrons and can be viewed as the electron density increase or redistribution. For simplicity, we assume the conductivity in the conductive region (filament) is constant. The motion of ions causes the change of the electron densities in transition and insulating regions, resulting in the formation, growth, and dissolution of the filaments. Since the TiO_2-TiO_{2-x} device is stable when no voltage bias is applied, we can model the ion motion by considering only the external electric field.[32] The internal temperature of the device, which leads to the fluctuations of cycle-to-cycle switching, is not included in our model. Without loss of generality, we assume the endpoint of the filament starts moving from the left end of the device ($x = 0$) at time 0. $n_t(x,t)$ is the electron density at the position x in the transition region at time t. Compared to the electron density n_c at the boundary between the conductive region and the transition region, the change of the electron density at x is $n_c - n_t(x,t)$, which is mainly due to the oxygen ion vacancy redistribution.[33]

When external voltage is applied, the electron densities are changing with time in both transition and insulating regions (filament growth). The electron density increment in an infinitesimal time interval dt equals the difference between the electron densities at positions $x - dx$ and x, or

$$\begin{aligned} n_t(x - dx, t) - n_t(x,t) &= \frac{dn_t(x,t)}{dx}(-dx) \\ &= -\frac{dn_t(x,t)}{dx} v(x,t) dt \\ &= \gamma_t (n_c - n_t(x,t)) E_t(x,t) dt. \end{aligned} \tag{9}$$

Here, γ_t is the electron generating coefficient in the transition region. Note that the maximum reachable electron density in the memristor device is n_c, or the region is fully conductive.

Based on Eq. (9), the growth velocity at position x can be calculated by

$$v(x,t) = -\frac{\gamma_t (n_c - n_t(x,t)) E_t(x,t)}{\frac{dn_t(x,t)}{dx}}, \tag{10}$$

where $\frac{dn_t(x,t)}{dx}$ can be derived from Eqs. (2) and (5).

The motion of the transition region can be described by the *average* growth velocity, which is defined as

$$\bar{v}(t) = \frac{\int_w^{w+\lambda} v(x,t)dx}{\lambda}. \tag{11}$$

This result shows that the filament growth is triggered by mainly the external electric field and can be viewed as the combined imaginary surfaces within the transition region. In the following sections, we simplify the expressions of n_c, $n_t(x,t)$, and $n_i(t)$ as n_c, n_t, and n_i, which are still the functions of x and/or t.

Substituting Eqs. (2) and (5) into Eq. (10), we have

$$v(x,t) = \left(\frac{n_c}{n_t} - 1\right) n_c E_c(t) \cdot \frac{\gamma_t}{n_t^2} \frac{\lambda n_c n_i}{n_c - n_i}. \tag{12}$$

Substituting Eqs. (2), (5), (7), and (12) into Eq. (11), the filament growth velocity $\frac{dw(t)}{dt}$ can be approximated by

$$\frac{dw(t)}{dt} \approx \bar{v}(t) = \gamma_t \lambda \beta \cdot \frac{1}{\frac{n_c}{n_i} - 1} \cdot \frac{V(t)}{w\left(1 - \frac{n_c}{n_i}\right) + \frac{1}{2}\lambda + \frac{n_c}{n_i}\left(D - \frac{1}{2}\lambda\right)}. \tag{13}$$

Here, β equals $\frac{1}{4}\left(\frac{n_c}{n_i} - 1\right)^3 + \frac{2}{3}\left(\frac{n_c}{n_i} - 1\right)^2 + \frac{1}{2}\left(\frac{n_c}{n_i} - 1\right)$.

The resistance/memristance of the memristor can be calculated by

$$R(t) = \frac{V(t)}{J_c A} = \frac{V(t)}{n_c q \mu E_c(t) A}. \tag{14}$$

Here, A is the cross section area of the memristor filament. Equations (13) and (14) describe the dynamic changes of memristor device structure and electrical property, respectively.

Assuming n_c and n_i are constant during the switching of the memristor (for example, the applied voltage magnitude is low or the programming pulse width is short), we can obtain the general form of w under a constant applied voltage V by integrating both sides of Eq. (13) as

$$w(t) = \frac{1}{1 - \frac{n_c}{n_i}} \left\{ \sqrt{\left[\left(1 - \frac{n_c}{n_i}\right) w(t_0) + C_0\right]^2 - 2\gamma_t \beta \lambda V \Delta t} - C_0 \right\}. \tag{15}$$

Here, $\Delta t = t - t_0$ and $C_0 = \frac{1}{2}\lambda + \frac{n_c}{n_i}\left(D - \frac{1}{2}\lambda\right)$. Equation (15) provides an analytical approximation on the growth of the filaments in the memristor. The internal state variable w is the expression of electron densities and the previous value of w_0. This result bridges two state variables at two different times under one fixed voltage. w represents the filament length, or the state of the device and is able to calculate the state variable value or the total resistance. As we shall see later, this analytical result is close to the experimental result of the total device resistance. Based on that, we can quickly estimate the memristor switching time in the following two scenarios:

If the device is switched on, or the filament is formed from the left-end of the memristor to the right-end, at $t_0 = 0$ (or $w(t_0) = 0$), Eq. (15) can be simplified as

$$w(t) = \frac{1}{1 - \frac{n_c}{n_i}} \left\{ \sqrt{C_0^2 - 2\gamma_t \beta V \lambda t} - C_0 \right\}. \tag{16}$$

The memristor switching time can be estimated by assuming $C_0^2 - 2\gamma_t \beta V \lambda t = 0$, or

$$t_{on} = \frac{C_0^2}{2\gamma_t \beta V \lambda}. \tag{17}$$

The corresponding portion of transition region at t_0 is $w(t_{on}) \approx D - \frac{1}{2}\lambda$ since $n_i \ll n_c$. Considering normally $\lambda \ll D$, it indicates that the filament is formed completely at the right end of the memristor at $t = t_{on}$, or the device is totally switched on.

Similarly, if the filament is in the dissolution process starts from the right-end of the memristor at $t_0 = 0$ (or $w(0) = D$), Eq. (15) can be simplified as

$$w(t) = \frac{1}{1 - \frac{n_c}{n_i}} \left\{ \sqrt{\left[\left(1 - \frac{n_c}{n_i}\right) D + C_0\right]^2 - 2\gamma_t \beta \lambda V t} - C_0 \right\}. \tag{18}$$

The time required to switch off the memristor (t_{off}) can be derived by assuming $w(t_{off}) = 0$, or

$$t_{off} = \frac{\left[\left(1 - \frac{n_c}{n_i}\right) D + 2C_0\right]\left(1 - \frac{n_c}{n_i}\right) D}{2\gamma_t \beta \lambda V}. \tag{19}$$

Table I summarized the three types of the device parameters used in our model, including the geometric parameters, the electrical parameters, and the structural parameters. The electron generating coefficients γ_t and γ_i are derived from the measured data and assumed constant for the different working ranges, as shown in Fig. 2. We compared our model with the experimentally obtained characterized static I-V curve and dynamic pulse programming curve of a TiO_2-TiO_{2-x} memristor device.

Fig. 2 shows the measured I-V curve from a real memristor device as well as the experimental data from the numerical simulation and analytical approximation. During the measurement, a sequence of voltage pulses is applied on the memristor device. The magnitude of the voltage pulse grows exponentially, and varies from positive to negative following *sine* function. The numerical simulation well fit the measured data in all four working ranges. The analytical approximation shows slight discrepancy from the measured data when the resistance is high. It is because the simulated

TABLE I. Modeling parameters.

	Parameters	Value	Parameters	Value
Geometric	D	35 nm	A	0.25 μm^2
Electrical	e	$1.602 \times 10^{-19} C$	n_c	8.75×10^{22} m^{-3}
Structural	w_0	0.15 D	λ_0	0.05 D
Working range		Derived parameters		
$1 \rightarrow 2$	γ_t	2.3×10^{-6}	γ_i	1×10^{-6}
$2 \rightarrow 1$		8×10^{-6}		1×10^{-8}
$1 \rightarrow 3$		1×10^{-10}		1×10^{-9}
$3 \rightarrow 1$		7×10^{-7}		2×10^{-7}

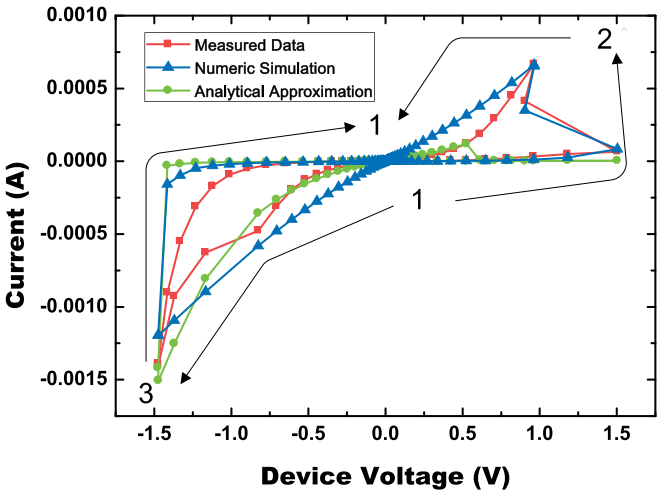

FIG. 2. Model validation with static I-V curve, including numerical simulation and analytical approximation. The magnitude of the applied voltage grows exponentially and follows *sine* function. The memristor is initially set to high resistance state.

filament growth velocity is lower than the actual value when the variation of n_i over time is ignored.

To prove the capability of our model on simulating the dynamic switching property of the memristor, we plot the resistance changes following the programming pulses in Fig. 3. The resistance of the memristor first decreases when the positive pulses are applied, and then raises when the polarization of the pulses changes to negative. Our numerical simulation matches the measured data very well over most of the plotted points. Small discrepancies show at the high resistance state. One reason for the deviations could be the impact of thermal fluctuations, which become prominent under a relatively low programming voltage. The analytical approximation shows relative large deviation from the measured data at the high-resistance state.

We proposed a compact model to simulate the transition region motion in the TiO_2-TiO_{2-x} memristor based on the classic ion transportation theory. Our model is validated with the measured data from a real TiO_2/TiO_{2-x} memristor device and proved capable of simulating the static and dynamic switching properties of the device with good accuracy. Our future work will focus on modeling the impact of temperature and 3-D model. We also plan to publish the corresponding Verilog-A model in the public domain in the near future.

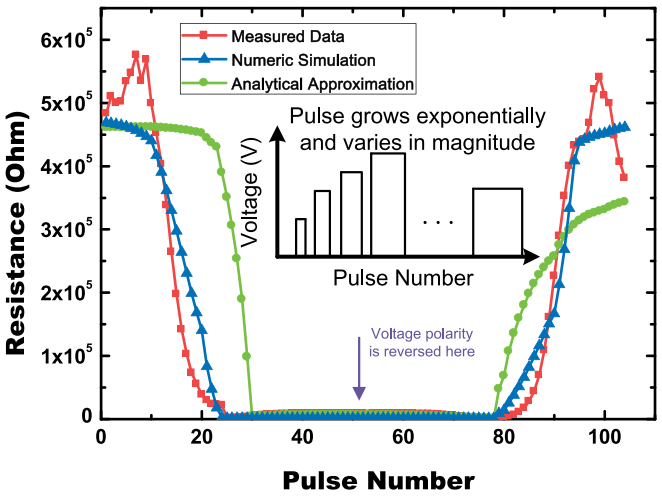

FIG. 3. Model validation with memristor dynamic switching for one single cycle, including numerical simulation and analytical approximation.

[1]D. B. Strukov, G. S. Snider, D. R. Stewart, and R. S. Williams, Nature **453**(7191), 80–83 (2008).
[2]D.-H. Kwon, K. M. Kim, J. H. Jang, J. M. Jeon, M. H. Lee, X.-S. Li, G.-S. Park, B. Lee, S. Han, M. Kim, and C. S. Hwang, Nat. Nanotechnol. **5**(2), 148–153 (2010).
[3]R. Waser, R. Dittmann, G. Staikov, and K. Szot, Adv. Mater. **21**(25–26), 2632–2663 (2009).
[4]J. J. Yang, M. D. Pickett, X. Li, D. A. A. Ohlberg, D. R. Stewart, and R. S. Williams, Nat. Nanotechnol. **3**(7), 429–433 (2008).
[5]S.-G. Park, B. Magyari-Kope, and Y. Nishi, IEEE Electron Device Lett. **32**(2), 197–199 (2011).
[6]S. Menzel, M. Waters, A. Marchewka, U. Böttger, R. Dittmann, and R. Waser, Adv. Funct. Mater. **21**(23), 4487–4492 (2011).
[7]W. Wang, S. Fujita, and S. S. Wong, IEEE Electron Device Lett. **30**(7), 763–765 (2009).
[8]W. Wang, S. Fujita, and S. S. Wong, IEEE Electron Device Lett. **30**(7), 733–735 (2009).
[9]F. Miao, J. J. Yang, J. Borghetti, G. Medeiros-Ribeiro, and R. S. Williams, Nanotechnology **22**(25), 254007 (2011).
[10]S. Kim, H. Y. Jeong, S.-Y. Choi, and Y.-K. Choi, Appl. Phys. Lett. **97**, 033508 (2010).
[11]C. Cagli, F. Nardi, and D. Ielmini, IEEE Trans. Electron Devices **56**(8), 1712–1720 (2009).
[12]D. Ielmini, IEEE Trans. Electron Devices **58**(12), 4309–4317 (2011).
[13]D. B. Strukov, J. L. Borghetti, and R. S. Williams, Small **5**(9), 1058–1063 (2009).
[14]S. Yu, X. Guan, and H.-S. Wong, in *2011 IEEE International Electron Devices Meeting (IEDM)* (IEEE, 2011), pp. 413–416.
[15]U. Russo, D. Ielmini, C. Cagli, and A. L. Lacaita, IEEE Trans. Electron Devices **56**(2), 186–192 (2009).
[16]D. Ielmini, F. Nardi, and S. Balatti, IEEE Trans. Electron Devices **59**(8), 2049–2056 (2012).
[17]G. Bersuker, D. Gilmer, D. Veksler, J. Yum, H. Park, S. Lian, L. Vandelli, A. Padovani, L. Larcher, K. McKenna *et al.*, in *2010 IEEE International Electron Devices Meeting (IEDM)* (IEEE, 2010), pp. 456–459.
[18]S. Long, C. Cagli, D. Ielmini, M. Liu, and J. Suñé, J. Appl. Phys. **111**(7), 074508 (2012).
[19]G. Bersuker, D. Gilmer, D. Veksler, P. Kirsch, L. Vandelli, A. Padovani, L. Larcher, K. McKenna, A. Shluger, V. Iglesias *et al.*, J. Appl. Phys. **110**(12), 124518 (2011).
[20]H. Y. Jeong, J. Y. Lee, and S.-Y. Choi, Appl. Phys. Lett. **97**(4), 042109 (2010).
[21]K. Kamiya, M. Young Yang, S.-G. Park, B. Magyari-Kope, Y. Nishi, M. Niwa, and K. Shiraishi, Appl. Phys. Lett. **100**(7), 073502 (2012).
[22]S. K. Kim, K. M. Kim, D. S. Jeong, W. Jeon, K. J. Yoon, and C. S. Hwanga, J. Mater. Res. **28**(3), 313–325 (2013).
[23]J. P. Strachan, M. D. Pickett, J. J. Yang, S. Aloni, A. David Kilcoyne, G. Medeiros-Ribeiro, and R. Stanley Williams, Adv. Mater. **22**(32), 3573–3577 (2010).
[24]S. Yu, X. Guan, and H.-S. P. Wong, Appl. Phys. Lett. **99**, 063507 (2011).
[25]B. Gao, B. Sun, H. Zhang, L. Liu, X. Liu, R. Han, J. Kang, and B. Yu, IEEE Electron Device Lett. **30**(12), 1326–1328 (2009).
[26]A. Makarov, V. Sverdlov, and S. Selberherr, J. Vac. Sci. Technol. B **29**(1), 01AD03 (2011).
[27]D. Li, M. Li, F. Zahid, J. Wang, and H. Guo, J. Appl. Phys. **112**(7), 073512 (2012).
[28]S. Savelev, A. Alexandrov, A. Bratkovsky, and R. Stanley Williams, Appl. Phys. Lett. **99**(5), 053108 (2011).
[29]S. Savelev, A. Alexandrov, A. Bratkovsky, and R. S. Williams, Nanotechnology **22**(25), 254011 (2011).
[30]M. D. Pickett, D. B. Strukov, J. L. Borghetti, J. J. Yang, G. S. Snider, D. R. Stewart, and R. S. Williams, J. Appl. Phys. **106**(7), 074508 (2009).
[31]J. D. Jackson, *Classical Electrodynamics*, 3rd ed. (Wiley, New York, 1998).
[32]D. B. Strukov and R. Stanley Williams, Appl. Phys. A **94**(3), 515–519 (2009).
[33]J. J. Yang, F. Miao, M. D. Pickett, D. A. A. Ohlberg, D. R. Stewart, C. N. Lau, and R. S. Williams, Nanotechnology **20**(21), 215201 (2009).